# *CHAPTER IV*

## *Pd/Cu bimetallic nanoparticles embedded in macroporous ion-exchange resins: An excellent heterogeneous catalyst for the Sonogashira reaction*

## IV.1. Introduction

Bronze is an alloy of copper and tin was the oldest record of a man-made bimetallic material, aimed to improving the performance of each of its two components. The bimetallic age of catalysis has taken a bit longer to come out, but it is now here pursuing the same purpose: better performance and new applications.

The field of heterogeneous catalysis, with particular emphasis on catalysis involving bimetallic nanomaterials (BNMs) that contain two different materials in the same nanoparticle, has seen many advances over the past few years. Significant progress has been made with regard to the preparation and characterization of a variety of different BNMs with well defined size, shape, and composition properties.[1]

Bimetallic nanoparticles (NPs), with two different metals, often show improved catalytic performances and find applications in several industrial processes, primarily in fuel industries or environmental catalytic processes, and more recently in C−C cross–coupling reactions.[2] Bimetallic catalysts represent an interesting class of catalysts because one metal can tune and/or modify the catalytic properties of the other due to the electronic and structural interactions.[3] They are also of importance because of the modification in their surface electrons relative to that of the individual metals.[4] There has been considerable interest in the formation, structure and further exploitation of the catalytic activity of bimetallic particles.[5] It has been often seen that metals interacting with either another metal or metal oxide at the nano level can form nanocomposites with superior activities not seen in bulk alloys.[6] From the standpoint of the reduction of environmental burdens and cost effectiveness, nanometal catalysts embedded in/on insoluble supports with ligand-free and minimal or no leaching are highly desirable. However, procedural simplicity, uniform dispersion, cheaper and robust polymeric surface, higher efficiency and life-cycle remain the major challenges for a heterogeneous catalyst.

Since several metal-catalyzed cross–coupling reactions require the presence of another metal either as a cocatalyst or to help control the overall process. Representative examples include: (i) Pd-catalyzed Heck coupling reaction in the presence of Ag salts, that is believed to occur via cationic mechanism and often has a profound effect in controlling the regio- and stereochemistry of the coupled product,[7] (ii) Sonogashira reaction between an aryl halide and terminal alkynes requires a combination of Pd and Cu as the catalysts, where $Cu^{+}$ plays a catalytic role in transferring the alkynyl group to Pd,[8] (iii) in the Stille coupling reaction, the accelerating effect of CuI on the Pd-catalyzed coupling of aryl iodide and organostannane derivative has been quantitatively evaluated.[9]

Since in early 1990s, bimetallic Pd nanoparticles have received widespread attention because of their extensive use in hydrogenation reactions, C−H bond activation, C−C coupling reactions and environmental catalytic processes. In 1996 Reetz et al. observed that the presence of tetraalkylammonium salts can lead to nanostructured $R_4N^+X^-$-stabilized bimetallic cluster Pd/Ni, having better catalytic activity than corresponding Pd clusters. The excellent redox properties of the Pd/Cu system and the pronounced "Cu-effect" in the Pd-catalyzed cross–coupling reaction stimulate the development of several heterogeneous bimetallic composites.[10]

**IV.2. Present work: Background and Objective**

Palladium-copper bimetallic catalysts have excellent properties both for oxidation reaction reactions and for catalysis in reducing atmospheres. They in fact are of interest as catalyst for the oxidation of CO[11a] and for the oxygen-assisted water gas shift reaction,[11b] and the selective hydrogenation of dienes to olefins.[11c] Several previous studies have been devoted to the characterization of similar materials by different techniques.[12] Copper enrichment has been reported in the case of Pd-Cu/$SiO_2$ catalyst used for dehydrochlorination of 1,2-dichloroethane[12h] and in optical materials.[12i]

Recent report shows monodisperse bimetallic Pd–Cu nanoparticles with controlled size and composition were synthesized by a one-step multiphase ethylene glycol (EG) method.[13] The as prepared nanoparticles were loaded onto a Vulcan XC-72 carbon support. Supported Pd–Cu nanomaterials showed enhanced electrocatalytic activity towards methanol oxidation compared with supported Pd nanoparticles. The solid–solution alloy structures in the bimetallic catalyst played a key role in improving the electrochemical activity.

After that Chang and their group have demonstrated a facile approach for the preparation of PdCu bimetallic NPs with various morphologies through a surfactant-assisted growth at 95 $^oC$.[14] This material was successfully applied in methanol oxidation reaction (MOR) in alkaline media. Upon increasing the copper content, the catalytic activity toward the MOR increases, mainly due to the advantages of the electroactive surface area.

Müslehiddinoglu et al.[15] developed a Pd-Cu/C catalyst as an alternative to Raney Ni for the highly diastereoselective hydrogenation of imines prepared from prochiral ketones and *α*-phenylethylamines (Scheme IV.1). These results revealed that chiral amines could be obtained with a diastereomeric excess (de) up to 94% using Pd-Cu/C, whereas conventional Pd/C catalysts only afforded a de of 72%. Further investigation revealed that a Pd:Cu ratio of 4:1 was required for a robust process.

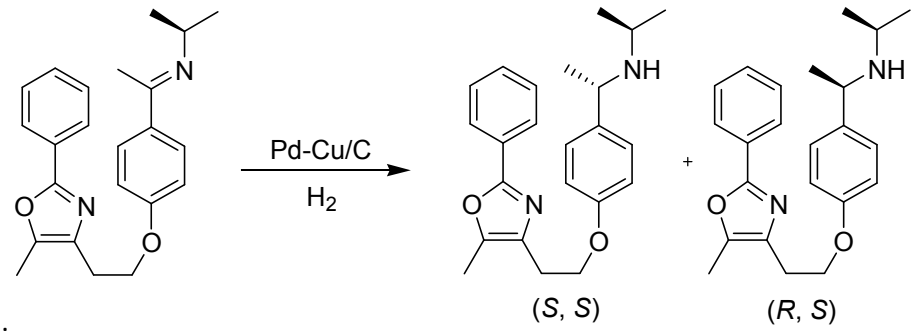


**Scheme IV.1.** Catalytic hydrogenation by Pd-Cu/C.

Palladium and copper exchanged montmorillonite K10 clay has been found to catalyse very efficiently the reaction between aryl halides (X = Br, I) and acrylates, and styrenes producing alkyl (*E*)-cinnamates and (*E*)-stilbenes respectively in high yields (Scheme IV.2).[16] The catalyst was recovered by simple filtration and reused up to three times without losing its activity.

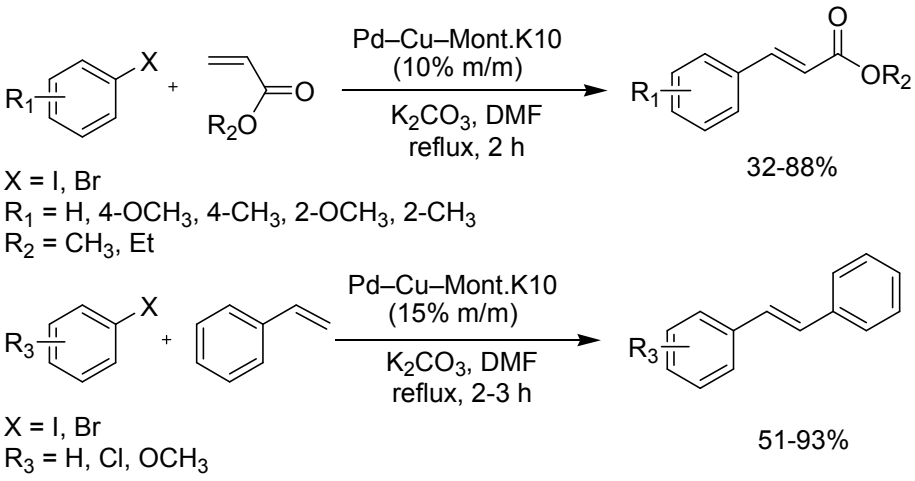


**Scheme IV.2.** Heck reaction using Pd–Cu–Mont.K10.

Another carbon-supported bimetallic Pd-M (M = Ag, Ni, and Cu) composites have been synthesized by Choi et al.[17] through $\gamma$-irradiation at room temperature, and the resulting Pd-Cu/C nanoparticles exhibited high catalytic efficiency in the Suzuki- and Heck-type coupling reactions.

Heshmatpour and their group have synthesized spherical metal NPs (Pd, Ag, Pd/Ag, Pd/Ni, and Pd/Cu) using a water-in-oil microemulsion system of water/dioctyl sulfosuccinate sodium salt (aerosol-OT, AOT)/isooctane at 25 $^oC$ based on the reverse micelle technique.[18] Among different combinations Pd/Cu (4:1) exhibits highest activity in the Heck reaction compare to other (Scheme IV.3). This catalyst was separated by centrifugation and used for recycling experiments. The activity of Pd catalyst was gradually decreased but the catalytic activity of Pd/Cu remains constant up to six consecutive runs.

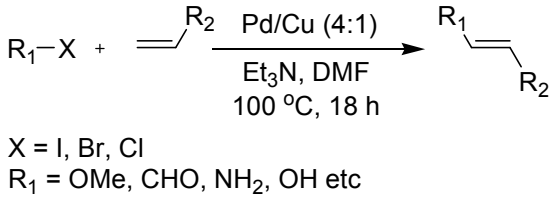


**Scheme IV.3.** Heck reaction of aryl halides with olefins catalyzed by Pd/Cu (4:1).

Very recently Gao et al.[19] have synthesized montmorillonite supported Pd-Cu nanoparticles (MMT@Pd/Cu), exhibits catalytic activity towards the Sonogashira coupling reaction using triphenylphosphine ($PPh_3$) as a ligand (Scheme IV.4). These catalysts were prepared on the basis of the unique metal ion adsorption capacity of montmorillonite and sequential reductive carbonylation via the thermolysis of *N*,*N*-dimethylformide. Kinetic studies revealed that the water-promoted swelling of the montmorillonite as well as the Pd-Cu bimetallic synergistic effect played a critical role in the high activity of the catalyst.

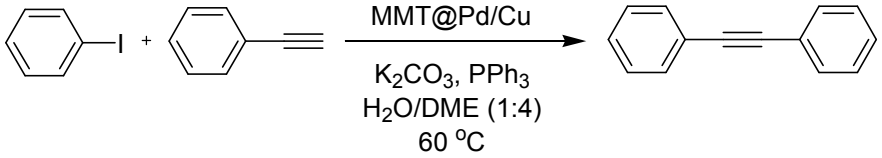


**Scheme IV.4.** MMT@Pd/Cu catalyzed Sonogashira coupling reaction.

Our previous lab report depicts the successful immobilization of Pd NPs on macroporous polystyrene-trimethylammonium anion-exchange resins and finds its application in various catalytic reduction and C−C coupling–coupling reactions.[20] However, to the best of our knowledge, there is no report available in the literature for the synthesis of bimetallic NPs impregnated on insoluble poly-ionic resins and to explore its heterogeneous catalytic activity in cross–coupling reactions. Here we report the synthesis and characterization of new class of heterogeneous Pd/Cu bimetallic composite NPs embedded on poly-ionic amberlite resins, which have shown efficient catalytic activity in the Sonogashira cross–coupling reaction under phosphine-ligand-free conditions with high recyclability.

## IV.3. Present work: Results and Discussion

### IV.3.1. Preparation of Heterogeneous Pd/Cu composite

Amberlite resin formate (ARF) was prepared from commercially available inexpensive Amberlite resin chloride by ion–exchange process as reported from this laboratory.[20,21] The resin beads were then washed with water followed by acetone, dried under vacuum and used for the preparation of heterogeneous bimetallic nanocomposites. Impregnation of bimetallic Pd/Cu on the ARF was performed by heating an equimolar mixture of solutions of palladium

acetate and cupric acetate in dimethylformamide (DMF) at different concentrations. Initial experiment using low concentration of each salt (0.033 mmol) afforded the composite material, which was denoted as Pd/Cu−ARF(I) and similar experiment using higher concentration of salts (0.25 mmol each) that furnished a new entity, denoted as Pd/Cu−ARF(II).

### IV.3.2. Characterizations of Pd/Cu−ARF

The morphology and microstructure of the samples were examined by FTIR spectroscopy, TEM equipped with EDS, powder XRD and AAS.

Initially we have focused on Pd/Cu−ARF(I). The AAS analysis shows nearly 90% of the added copper was present in it. The surface topopraphy and dispersion of active components over the ARF were examined by scanning electron microscopy (SEM) (Figure IV.1).

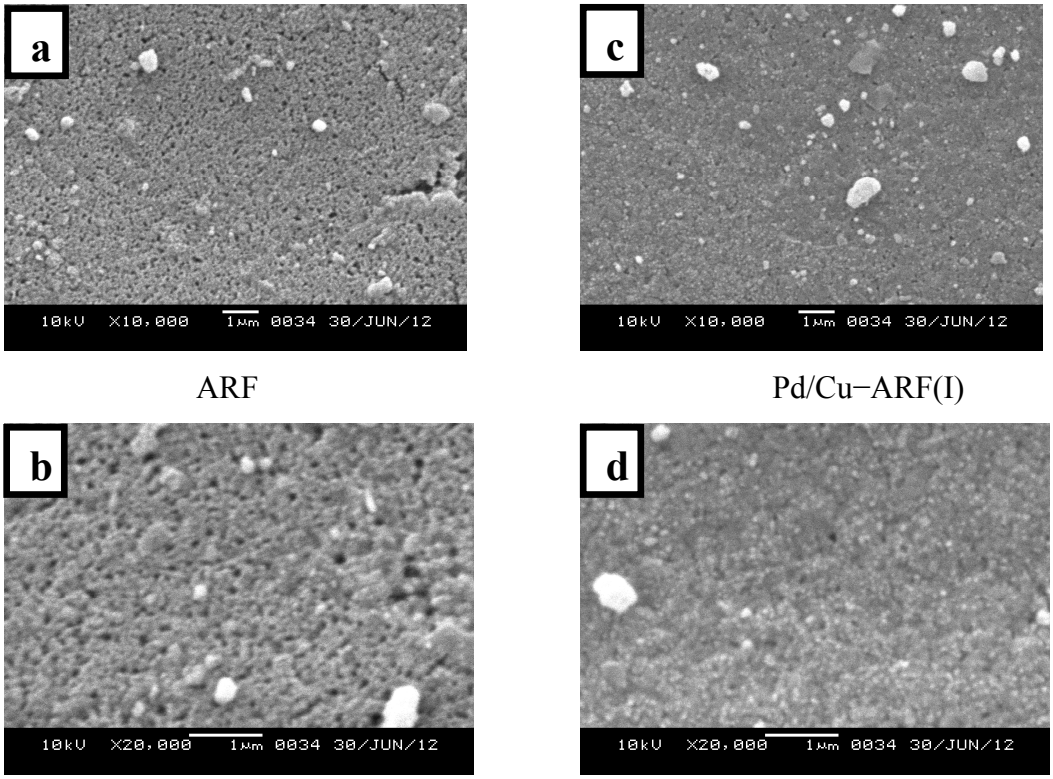


**Figure IV.1.** Scanning electron micrographs of ARF (a, b), Pd/Cu−ARF(I) (c, d) at different magnifications.

The powder XRD patterns of ARF and Pd/Cu−ARF(I) are presented in Figure IV.2. It is evident that the support (ARF) and supported bimetal at low concentration [Pd/Cu−ARF(I)] appeared almost identical and however showed no signature of NPs.

To understand the actual structural morphology of the composite material, Pd/Cu−ARF(II) was prepared and characterized in details.

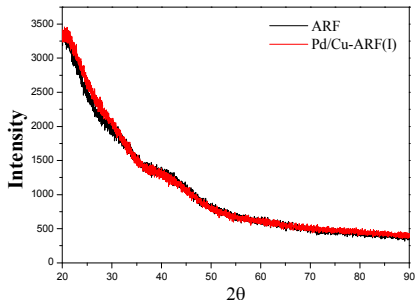


**Figure IV.2.** Powder XRD of ARF and the corresponding Pd-Cu incorporated resin (Pd/Cu−ARF(I)).

The FTIR spectra of bimetallic species were recorded in the range 4000–400 $cm^{-1}$ and compared with that of ARF. Figure IV.3 show the FTIR spectra in the range of 2000–400 $cm^{-1}$. While the carboxylate anion ($HCOO^{-}$) of the ARF exhibits both symmetric and anti-symmetric stretching vibrations respectively at 1346 and 1593 $cm^{-1}$, the composites Pd/Cu−ARF(I) and Pd/Cu−ARF(II) absorb at 1412 and 1655 $cm^{-1}$ for these vibrations. A clear shifting of the bands in the range of 60-65 $cm^{-1}$ was observed conforming to our previous studies with the monometallic Pd−ARF (Figure IV.3),[20] and suggesting possible electrostatic binding of the metallic species with the poly-ionic resins. It can also be noted from Figure IV.3 that an intense FTIR peak around 1575 $cm^{-1}$ is appeared in the case of Pd/Cu−ARF(II), which is almost absent in Pd/Cu−ARF(I). This may be assigned as a peak of $COO^{-}$, bonded with the metal in amberlite resin,[22] and appeared sharply in Pd/Cu−ARF(II) possibly due to the larger amount of metal doping.

The XRD patterns of amberlite resins formate, (ARF) and that of the corresponding Pd/Cu incorporated resins (Pd/Cu−ARF(II)) are shown in Figure IV.4. Here, we did not observe any signals related to the Pd- and Cu-acetate, indicating complete decomposition of the salts in the case of Pd/Cu−ARF(II). The impregnated resins Pd/Cu−ARF(II) (dried at 60 °C) exhibited Bragg diffractions corresponding to the cupric oxide (CuO), palladium oxide (PdO) and palladium (Pd), while the pure ARF showed amorphous characteristics. The peak positions are labelled in Figure IV.4. The corresponding JCPDS peak positions with relative intensities are also shown as green (PdO), blue (CuO) and pink (Pd) lines. The broad XRD pattern of Pd/Cu−ARF(II) suggested poor crystalline nature of the embedded materials. Nevertheless the existence of XRD peaks at 34.48, 46.16, 55.89 and 61.75° 2θ clearly suggested the PdO (002), (102), (112) and (103) planes, respectively (JCPDS#01-075-0200). The appearance of peaks at 40, ~46.5 and 67.91° 2θ indicated the presence of (111), (200) and (220) planes, respectively of fcc Pd (JCPDS#01-088-2335). Further, we found peaks near 35.39, 46.25, 57.91, 61.64° 2θ, which could be indexed as ($\bar{1}$11), ($\bar{1}$12), (202) and ($\bar{1}$13) of CuO, respectively (JCPDS#01-089-2531).

The TEM analysis of Pd/Cu−ARF(II) is presented in Figure IV.5. Low resolution TEM images showing nanoparticles embedded in resin matrix are shown in Figure IV.5a,b. The

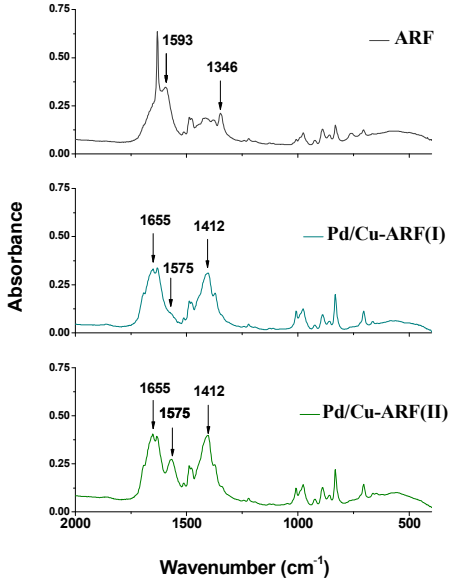


**Figure IV.3.** FTIR spectra of the ARF and bimetallic composites [Pd/Cu−ARF(I) and Pd/Cu−ARF(II)].

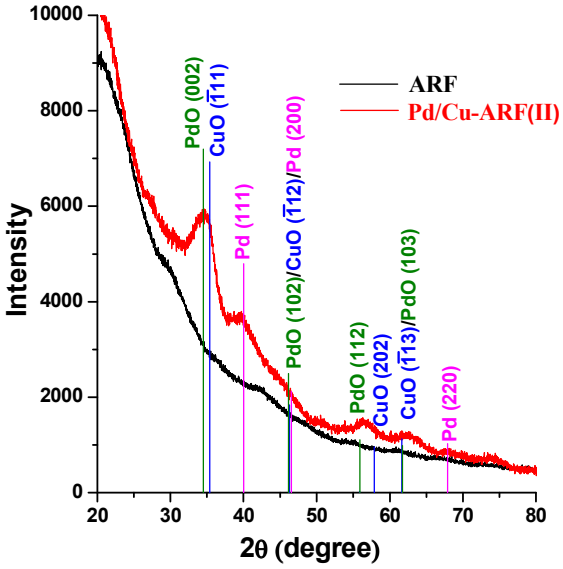


**Figure IV.4.** High angle XRD patterens of ARF and bimetallic composite Pd/Cu−ARF(II).

presence of diffused ring as well as spots corresponding to the Pd(111), PdO (002) and CuO ($\bar{1}$11) in the SAED (inset of Figure IV.5a) indicate existence of crystalline NPs, which is also supported by the XRD pattern (Figure IV.4). We magnified a small portion of Figure IV.5a for clarification and presented it as Figure IV.5b. It shows homogeneous distribution of NPs throughout the matrix. Figure IV.5c shows the particle size distribution, estimated from Figure IV.5b, and the mean diameter of the particle was found to be ~4.9 nm. Energy dispersive X-ray scattering (EDX) analysis of Pd/Cu-ARF(II) (Figure IV.5d) confirmed the presence of Pd, Cu and O and C in the sample. To understand the structure of the NPs, high resolution TEM (HRTEM) studies were undertaken using field emission gun (FEG) transmission electron microscope and results are presented in Figure IV.5e-f. Figure IV.5e shows NPs with clear crystalline fringe patterns. Magnified view of a representative NP (marked by 'A' in Figure IV.5e) is shown in Figure IV.5f with labelling of characteristic fringes. The Fourier diffractogram (FFT) obtained from (IV.5e) is shown in Figure IV.5g. The co-existence of Pd (111) and PdO/CuO lattice spacings are clearly observed in the NPs (Figure IV.5f,g). Thus, HRTEM studies as well as SAED revealed the composite nature of NPs.

From XRD and TEM analysis, we can thus say that composite NPs, made of Pd/PdO/CuO, have been embedded in the poly-ionic amberlite resins. The CuO might be formed by the ox-

idation of initially formed Cu(0) NPs, as also observed previously in the preparation of other

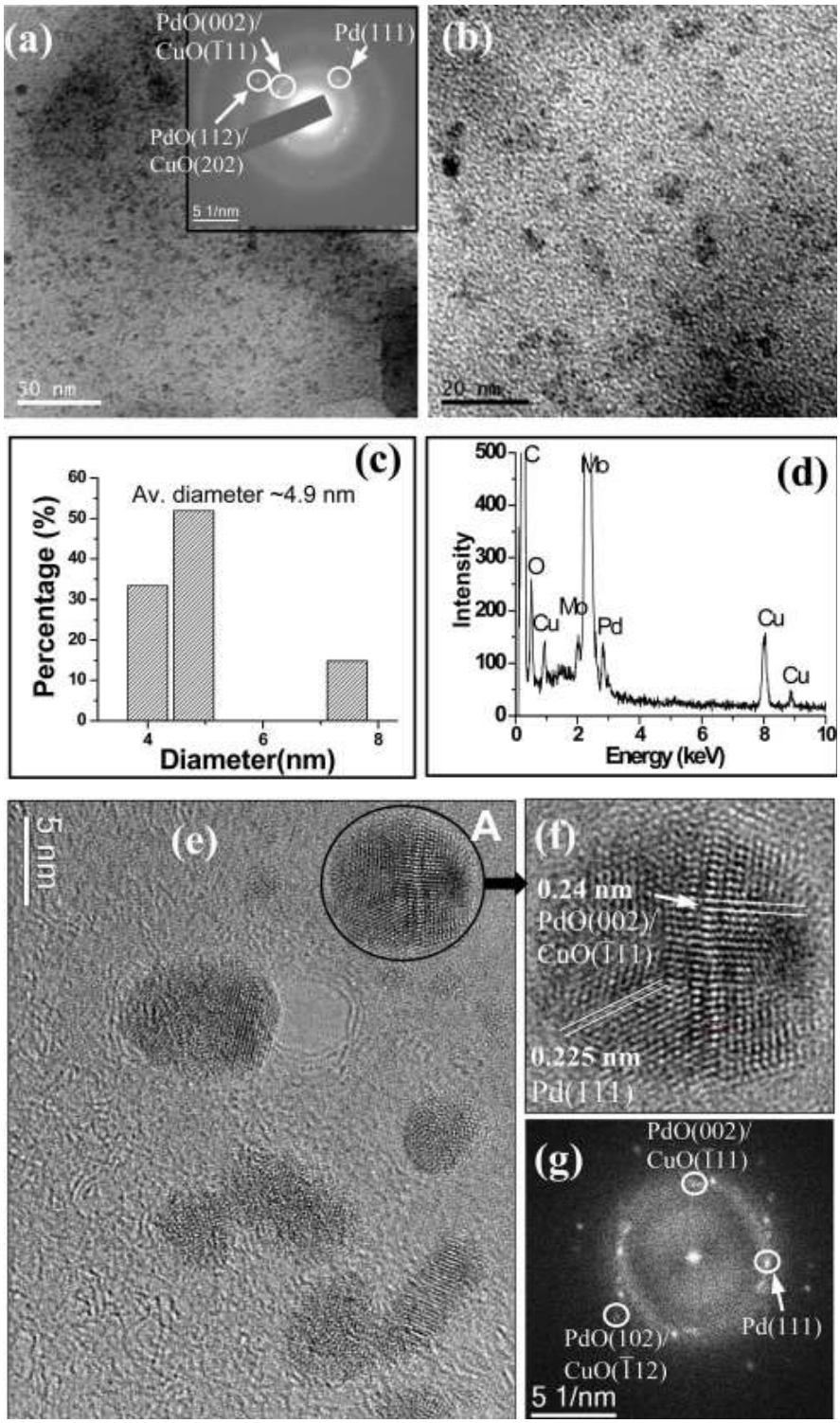


**Figure IV.5.** (a) Bright field low resolution TEM images of Pd/Cu−ARF(II); the inset shows the selected area electron diffraction (SAED) pattern; (b) representation of the magnified view of a small portion of (a); (c) particle size distribution evaluated from (b); (d) EDX pattern of the sample showing the existence of elemental C (very strong), O, Pd and Cu; a part of C and very strong Mo signals are from the carbon coated Mo grid used for the TEM study; (e) high resolution TEM image showing crystalline NPs; (f) magnified view of the NP marked by 'A' in (e); (g) Fourier diffractogram taken from (e).

heterogeneous bimetallic Cu-M nanocomposites.[23] Total copper present in the heterogeneous nanocomposite material, Pd/Cu−ARF(II) has been estimated by the AAS. For this purpose 50 mg of the sample was digested with concentrated $HNO_3$ (1 mL) and analysed. From such analysis Cu content has been estimated to be 0.205 mmol $g^{-1}$ of the Pd/Cu−ARF(II).

### IV.3.3. Catalytic Activity of Pd/Cu−ARF(II)

The metal-catalyzed $sp^2$–sp coupling reaction between aryl or alkenyl halides and terminal alkynes, known as the Sonogashira reaction,[24] is one of the most important reactions for the formation of C−C bonds in organic synthesis.[25] Combination of Pd and Cu salts along with suitable phosphine ligands as the catalytic system for such cross–coupling reactions of $sp^2$-C halides with terminal acetylenes requires careful choice of substrates and skilful tailoring of the reaction conditions.[26] Competing homo-coupling of terminal alkynes in the presence of Pd/Cu catalysts remain one of the major side reactions, which is often avoided or minimized by conducting the Sonogashira reaction under a blanket of $N_2$ or a mixture of $N_2$ and $H_2$.[27] On the other hand, few successful examples of copper-free Sonogashira coupling require expensive aminophosphine ligands.[28] We optimized the reaction conditions with 4-iodotoluene and propargyl acetate using the newly developed heterogeneous combination of Pd/CuO nanocomposites, and the best conversion was achieved in the presence of $K_2CO_3$ as the base in $CH_3CN$ solvent at 80 °C under $N_2$ for 12h. As regard to the amount of the catalysts, it was observed that 100 mg $mmol^{-1}$ was sufficed to catalyze the process. To explore the scope and limitations of the catalyst, a range of substituted iodoarenes was tested and found to undergo Sonogashira coupling with different aliphatic and aromatic alkynes (Scheme IV.5). The results are presented in Table IV.1. The cross–coupling with electron-rich aryl bromides was not successful, though hetero-aromatic bromide such as 3-bromoquinoline or electron-deficient bromoarenes gave the corresponding coupled product in excellent yield.

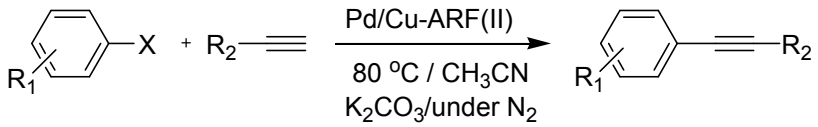


**Scheme IV.5.** Sonogashira cross–coupling in the presence of Pd/Cu−ARF(II).

Poor catalytic activity with deactivated aryl bromide in Sonogashira coupling has been exploited with a suitable example. 1-Bromo-3-iodobenzene showed excellent chemoselectivity when the Sonogashira coupling with 4-tolyl acetylene was carried out in the presence of Pd/Cu−ARF(II) to obtain selectively 1-(2-(3-bromophenyl) ethynyl)-4

methylbenzene in 92% yield (Table IV.1, entry 12A). Subsequently, the same catalytic system was used for Suzuki–Miyaura coupling with phenylboronic acid to obtain 1-(2-(3 biphenyl)ethynyl)-4-methylbenzene in 81% yield (Table IV.1, entry 12B). This reaction established that the catalytic system, Pd/Cu−ARF(II), is effective for the Suzuki–Miyaura cross–coupling reaction as well.

**Table IV.1.** Sonogashira coupling reactions of haloarenes with terminal alkynes in the presence of catalytic Pd/Cu−ARF(II).[a]

| Sl. No. | Ar-X | Alkyne | Time (h) | Product | Yield[b] (%) |
|---|---|---|---|---|---|
| 1 | 4- $H_3COC_6H_4I$ | $\equiv C_6H_5$ | 6 | 4- $H_3COH_4C_6-\equiv-C_6H_5$ | 85 |
| 2 | 4- $H_3CC_6H_4I$ | $\equiv CH_2OCOCH_3$ | 12 | 4- $H_3CH_4C_6-\equiv-CH_2OCOCH_3$ | 90 |
| 3 | 2- $H_3CC_6H_4I$ | $\equiv CH_2OCOCH_2CH_3$ | 10 | 2- $H_3CH_4C_6-\equiv-CH_2OCOCH_2CH_3$ | 87 |
| 4 | 3- $H_3COC_6H_4I$ | $\equiv CH_2CH_2C_6H_5$ | 6 | 3- $H_3COH_4C_6-\equiv-CH_2CH_2C_6H_5$ | 84 |
| 5 | 3- $NO_2C_6H_4I$ | $\equiv C_6H_5$ | 3 | 3- $NO_2H_4C_6-\equiv-C_6H_5$ | 95 |
| 6 | 3- $BrC_6H_4I$ | $\equiv CH_2OCOCH_2CH_3$ | 12 | 3- $BrH_4C_6-\equiv-CH_2OCOCH_2CH_3$ | 77 |
| 7 | 3- $ClC_6H_4I$ | $\equiv CH_2OCOCH_2CH_3$ | 12 | 3- $ClH_4C_6-\equiv-CH_2OCOCH_2CH_3$ | 78 |
| 8[c] | 3- $H_3CC_6H_4Br$ | $\equiv C_6H_5$ | 16 | No Reaction | - |
| 9 | 4- $H_3CCOC_6H_4Cl$ | $\equiv CH_2CH_2C_6H_5$ | 16 | No Reaction | - |
| 10 | 3- $C_9H_6NBr$ | $\equiv C_6H_5$ | 12 | 3- $C_9H_6N-\equiv-C_6H_5$ | 77 |
| 11 | 3- $NO_2C_6H_4Br$ | $\equiv C_6H_5$ | 10 | 3- $NO_2H_4C_6-\equiv-C_6H_5$ | 93 |
| 12A | 1-Br-3-$IC_6H_4$ | $\equiv C_6H_4(4\text{-}CH_3)$ | 6 | 1-Br-3-$C_6H_4-\equiv-C_6H_5(4\text{-}CH_3)$ | 92 |
| 12B[d] | 1-Br-3-$C_6H_4-\equiv-C_6H_5(4\text{-}CH_3)$ | $C_6H_5B(OH)_2$ | 6 | 1-$C_6H_5$-3-$C_6H_4-\equiv-C_6H_5(4\text{-}CH_3)$ | 81 |

[a]Pd/Cu−ARF(II) (100 mg), ArX (1 mmol), alkyl acetylene (1.1 mmol)/aryl acetylene (1.5 mmol), $K_2CO_3$ (1.5 mmol), MeCN (3 mL), heating the reaction at 80 $^oC$ under $N_2$. [b]Yields are for isolated pure compounds, characterized by mp, IR and NMR spectral data. [c]Homo-coupled diyne was isolated in 62% yield. [d]Suzuki–Miyaura cross–coupling reaction using same catalytic system, [Pd/Cu−ARF(II)], (see experimental).

Although the exact mechanism for the Sonogashira cross–coupling reaction is not known,[26a] the catalytic process may be considered to involve two parts: (i) $Pd^0$ undergoes oxidative addition to aryl halide, and (ii) $Cu^{+2}$ is *in situ* reduced to $Cu^{+1}$, which forms transient copper acetylide species. The process is then completed via transmetalation followed by reductive elimination to finally afford the cross–coupled product. We also examined Sonogashira coupling reaction in the presence of Pd/Cu−ARF(I), which is much less efficient as compared to Pd/Cu−ARF(II), producing the Sonogashira coupled product in 25-40% isolated yield.

### IV.3.4. Heterogeneity Test

#### IV.3.4.1. Hg(0) and $CS_2$ poisoning tests

The heterogeneity of the catalyst is often checked by catalyst-poisoning experiments, and addition of Hg(0) in the reaction medium to see any poisoning of the catalytic activity has been suggested by Whitesides,[29] and Crabtree,[30] followed by other groups.[31] Similar experiment was performed in Sonogashira coupling between 3-iodonitrobenzene and phenyl acetylene (1:1.5 mmol) in acetonitrile in the presence of Pd/Cu−ARF(II) (100 mg) and Hg(0) (250 mg) with gentle magnetic stirring at 80 °C. After heating the reaction mixture for 1h, it was analyzed by HPLC that showed the ratio of iodoarene and the coupled product in 67:33. The reaction was then continued for another 2h and now HPLC analysis showed complete conversion to the coupled product. Further experiment using excess Hg(0) (1.5 g, 340 equivalents per palladium) and stirring the reaction vigorously did not show suppression of catalytic activity, and complete conversion was observed after 3h. Although poisoning by elemental mercury is often used as a test for heterogeneous catalysis, this is not definitive probably in the context of metal-catalyzed coupling chemistries.[32] Poisoning experiment using ligand like $CS_2$ can also be powerful if performed quantitatively.[33] We therefore conducted catalyst poisoning tests in Sonogashira coupling between 3-iodonitrobenzene and phenyl acetylene by adding varying quantities of $CS_2$ to the reaction mixture. After about 15% conversion of the product (by HPLC), $CS_2$ was added and the reaction was continued for 3h to check the amount of conversion. Figure IV.6 shows the results of five independent experiments as a plot of % conversion (± 2−3%) to the cross coupled product as a function of amounts of $CS_2$ added. Near complete cessation of the Sonogashira coupling was observed with 1 mg of $CS_2$ (0.013 mmol) as against 0.022 mmol of the palladium (<1.0 eq), suggesting that the Pd/Cu−ARF(II) nanocomposites are indeed heterogeneous catalyst.

#### IV.3.4.2. Hot filtration test

Leaching of any metal from the resin-soaked heterogeneous surface was tested following the literature procedure.[30,34] Accordingly, the Sonogashira reaction mixture is filtered off to separate the solid catalysts after 1h in hot condition, and the filtrate was analyzed by HPLC (~33% conversion). The AAS analysis of the filtrate showed absence of any copper. The liquid phase was heated under reflux for another 3h in the absence of any added catalyst and subsequent HPLC analysis did not show further conversion, signifying that the metals are not leached out from the polymeric support during the first hour of the reaction.

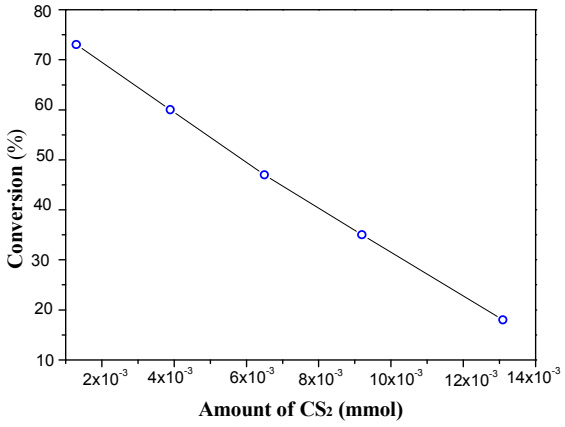


**Figure IV.6.** Plot of % conversions (± 2−3%) to the cross coupled product versus quantities of $CS_2$ (in mmol) used as the catalyst poisoning in Sonogashira reaction.

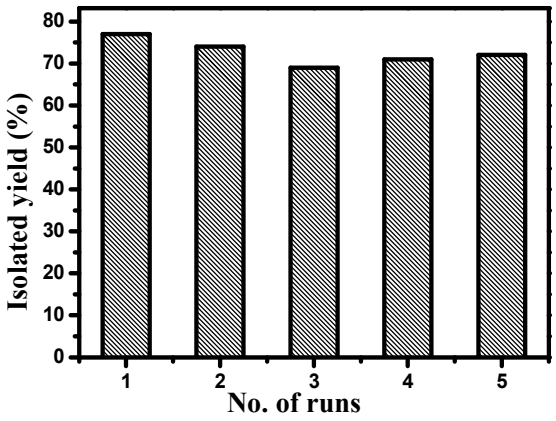


**Figure IV.7.** Recycling experiments using Pd/Cu−ARF(II) in the cross–coupling reaction between 4-iodotoluene and propargyl acetate.

### IV.3.5: Test for Recyclability

We also checked the reusability of Pd/Cu−ARF(II) in the reaction between 4-iodotoluene and propargyl acetate. After the reaction, resin beads were recovered from the reaction mixture by simple filtration, washed thoroughly with water followed by acetone, and then dried under vacuum. The recovered catalyst was reused four times without losing its activity (Figure IV.7).

## IV.4. Conclusion

In conclusion, a new class of poly-ionic resin-supported Pd/Cu based bimetallic nanocomposite has been synthesized, characterized and applied as the catalyst in Sonogashira cross–coupling reaction. The bimetallic nanoparticles composed of metallic Pd/PdO/CuO has found to be distributed very homogeneously throughout the polymeric matrix. The heterogeneous catalytic activity was examined by hot-filtration and metal-scavenger experiments and found to be highly efficient and recyclable at least for five consecutive runs. This Pd/Cu based nanocomposite catalytic system has been applied for the first time in Sonogashira cross–coupling reactions under ligand free conditions.

## IV.5. Experimental section

### IV.5.1. General information

Amberlite IRA 900 (chloride form) was purchased from Acros Organics, Belgium and used after washing with water and acetone followed by drying under vacuum. Other chemicals were purchased and used directly. FTIR spectra were recorded with a Nicolet 380 FTIR

spectrometer using KBr pellet method. NMR spectra were taken in $CDCl_3$ using Bruker Avance AV-300 spectrometer operating for $^1H$ at 300 MHz and for $^{13}C$ at 75 MHz. The spectral data were measured using TMS as the internal standard. AAS measurements were made using Varian SpectrAA 50B instrument. The X-ray diffraction (XRD) studies of the powder samples were done using the Rigaku SmartLab (9 kW) diffractometer using CuKα radiation. Transmission electron microscopy (TEM) of the samples were recorded with Tecnai G2 30ST (FEI Company) operating at 300 kV and JEOL JEM–2100F (FEG) operating at 200 kV. To prepare the TEM sample, a small amount of ground sample was first dispersed in acetone. Then one small drop of this dispersion was applied on a carbon-coated molybdenum grid.

The amberlite resin formate (ARF) was prepared from commercially available Amberlite IRA 900 (chloride form) (Source: Acros Organics, Belgium) by rinsing with 10% aqueous formic acid solution until free from chloride ions. The resin beads were then washed with water followed by acetone, dried under vacuum, and used for the preparation of heterogeneous bimetallic nanocomposites.

### IV.5.2. Preparation of Pd/Cu−AFR(I) & Pd/Cu−AFR(II)

**Pd/Cu−AFR(I)**

To a solution of $Pd(OAc)_2$ (7.5 mg, 0.033 mmol) and $Cu(OAc)_2$ (6.6 mg, 0.033 mmol) in DMF (3 mL) was added ARF (1 g) and the mixture taken in screw-capped sealed tube was heated at 60 $^oC$ for 1 h with occasional shaking. The supernatant liquid appeared completely colourless by this time and the greyish beads of ARF turned black. The mixture was cooled to room temperature and the resin beads were filtered off and washed with water (3 x 5 mL) and acetone (2 x 5 mL). Resulting black resin beads were dried under vacuum and used for analyses and reactions.

**Pd/Cu−AFR(II)**

Similar procedure was followed using a solution of $Pd(OAc)_2$ (56 mg, 0.25 mmol) and $Cu(OAc)_2$ (50 mg, 0.25 mmol) in DMF (10 mL) for the ARF (1 g).

### IV.5.3. Sonogashira cross–coupling reaction using Pd/Cu−ARF(II)

To a suspension of Pd/Cu−ARF(II) (100 mg) in acetonitrile (3 mL) were added aryl halide (1 mmol), acetylene (1.1 mmol for aliphatic alkynes and 1.5 mmol for aromatic alkynes) and $K_2CO_3$ (1.5 mmol). The reaction mixture was then heated under $N_2$ with gentle magnetic stirring for hours, as mentioned in the Table IV.1 and monitored by tlc. After cooling, the mixture was diluted with water (5 mL), and filtered through a cotton bed. The filtrate was

extracted with diethyl ether (3 x 10 mL) and the combined organic extracts were washed with brine (5 mL), dried over sodium sulphate and concentrated under vacuum. The residue was purified by passing through a short silica gel column and elution with light petroleum or 2% ethyl acetate-light petroleum. All products were characterized by $^{1}H$, $^{13}C$ NMR and FTIR spectral data, and also compared with reported melting point (for known solid compounds).

### IV.5.4. Suzuki–Miyaura cross–coupling reaction using Pd/Cu−ARF(II) (Table IV.1, entry 12B)

A mixture of 1-(2-(3-bromophenyl)ethyl)-4-methylbenzene (271 mg, 1 mmol), phenylboronic acid (134 mg, 1.1 mmol), $K_2CO_3$ (152 mg, 1.1 mmol) and the Pd/Cu−ARF(II) (150 mg) in DMF (3 mL) was heated at 90 $^{o}$C with occasional magnetic stirring. The reaction was monitored by tlc and after 6h, the mixture was cooled, diluted with water (5 mL) and extracted with diethyl ether (3 x 10 mL). The combined ethereal extracts was dried ($Na_2SO_4$) and evaporated to afford an oily residue. Column chromatography over silica gel and elution with light petroleum furnished the desired product, 1-(2-(3-biphenyl)ethynyl)-4-methylbenzene (217 mg, 81%). The product was characterized by NMR spectral data.

### IV.5.5. Physical properties and spectral data of compounds

**Table IV.1, entry 1**

**1-Methoxy-4-(2-phenylethynyl)benzene**[35]

White crystalline solid, mp 56-58 $^{o}$C (Lit. mp 58-60 $^{o}$C)

IR (in KBr): $\nu_{max}$ 2216 cm$^{-1}$

$^{1}H$ NMR ($CDCl_3$, 300 MHz): δ/ppm 3.82 (s, 3H, $OCH_3$), 6.86-6.89 (m, 2H, ArH), 7.31-7.33 (m, 3H, ArH), 7.45-7.53 (m, 4H, ArH); $^{13}C$ NMR ($CDCl_3$, 75 MHz): δ/ppm 55.3, 88.0, 89.3, 114.0, 115.4, 123.6, 127.9, 128.3, 131.4, 133.0, 159.6.

**Table IV.2, entry 2**

**3-*p*-Tolylprop-2-ynyl acetate**

Colourless liquid

IR (neat) $\nu_{max}$ 2237, 1747 cm$^{-1}$

$^{1}H$ NMR ($CDCl_3$, 300 MHz): δ/ppm 2.13 (s, 3H, C$\underline{H}_3$CO), 2.35 (s, 3H, ArC$\underline{H}_3$), 4.90 (s, 2H, $CH_2$), 7.12 (d, *J* = 8.1 Hz, 2H, ArH), 7.34 (d, *J* = 8.1 Hz, 2H, ArH); $^{13}C$ NMR ($CDCl_3$, 75 MHz): δ/ppm 20.8, 21.5, 52.9, 82.1, 86.6, 119.0, 129.0,131.8, 139.0, 170.4.

**Table IV.1, entry 3**

**3-*o*-Tolylprop-2-ynyl propionate**

Colourless liquid

IR (neat): $\nu_{max}$ 2229, 1743 $cm^{-1}$

$^1H$ NMR ($CDCl_3$, 300 MHz): δ/ppm 1.19 (t, *J* = 7.5 Hz, 3H, C<u>H</u>$_3$), 2.38-2.45 (m, 5H, ArC<u>H</u>$_3$, C<u>H</u>$_2$), 4.95 (s, 2H, O-$CH_2$), 7.10-7.26 (m, 3H, ArH), 7.41 (d, *J* = 7.5 Hz, 1H, ArH); $^{13}C$ NMR ($CDCl_3$, 75 MHz): δ/ppm 9.0, 20.6, 27.4, 52.8, 85.3, 86.8, 121.9, 125.5, 128.7, 129.4, 132.2, 140.5, 173.8.

**Table IV.1, entry 4**

**1-Methoxy-3-(4-phenylbut-1-ynyl)benzene**[20]

Colourless liquid

IR (neat): $\nu_{max}$ 2227 $cm^{-1}$

$^1H$ NMR ($CDCl_3$, 300 MHz): δ/ppm 2.69 (t, *J* = 7.5 Hz, 2H, $CH_2$), 2.92 (t, *J* = 7.5 Hz, 2H, $CH_2$-Ar), 3.78 (s, 3H, O-$CH_3$), 6.82-6.85 (m, 1H, ArH), 6.90-6.91 (m, 1H, ArH), 6.95-6.98 (m, 1H, ArH), 7.16-7.32 (m, 6H, ArH); $^{13}C$ NMR ($CDCl_3$, 75 MHz): 21.7, 35.1, 55.2, 81.2, 89.4, 114.2, 116.4, 124.0, 124.8, 126.3, 128.4, 128.5, 129.2, 140.7, 159.2.

**Table IV.1, entry 5**

**1-(2-(3-nitrophenyl)ethynyl)benzene**[33]

Yellow solid, 69-71 $^oC$ (Lit. mp 67-69 $^oC$)

IR (in KBr): $\nu_{max}$ 2207 $cm^{-1}$

$^1H$ NMR ($CDCl_3$, 300 MHz): δ/ppm 7.38-7.39 (m, 3H, ArH), 7.50-7.57 (m, 3H, ArH), 7.80-7.84 (m, 1H, ArH), 8.15-8.19 (m, 1H, ArH), 8.37-8.38 (m, 1H, ArH); $^{13}C$ NMR ($CDCl_3$, 75 MHz): δ/ppm 86.7, 91.9, 122.2, 122.9, 125.2, 126.4, 128.5, 129.0, 129.3, 131.8, 137.2, 148.2.

**Table IV.1, entry 6**

**3-(3-Bromophenyl)prop-2-ynyl propionate**

Colourless liquid

IR (neat): $\nu_{max}$ 2229, 1743 $cm^{-1}$

$^1H$ NMR ($CDCl_3$, 300 MHz): δ/ppm 1.18 (t, *J* = 7.5 Hz, 3H, $CH_3$), 2.41 (q, *J* = 7.5 Hz, 2H, C<u>H</u>$_2$-$CH_3$), 4.90 (s, 2H, O-C<u>H</u>$_2$), 7.15-7.21 (m, 1H, ArH), 7.36-7.39 (m, 1H, ArH), 7.45-7.48 (m, 1H, ArH), 7.60-7.61 (m, 1H, ArH); $^{13}C$ NMR ($CDCl_3$, 75 MHz): 8.9, 27.3, 52.4, 84.4, 84.7, 122.1, 124.1, 129.7, 130.4, 131.9, 134.6, 173.7.

**Table IV.1, entry 7**

**3-(3-Chlorophenyl)prop-2-ynyl propionate**

Colourless liquid

IR (neat): $\nu_{max}$ 2229, 1743 $cm^{-1}$

$^1H$ NMR ($CDCl_3$, 300 MHz): δ/ppm 1.18 (t, *J* = 7.2 Hz, 3H, $CH_3$), 2.40 (q, *J* = 7.5 Hz, 2H,

C$\underline{H_2}$-$CH_3$), 4.90 (s, 2H, O-C$\underline{H_2}$), 7.21-7.34 (m, 3H, ArH), 7.44 (s, 1H, ArH); $^{13}$C NMR ($CDCl_3$, 75 MHz): 8.9, 27.3, 52.4, 84.3, 84.8, 123.8, 128.9, 129.5, 129.9, 131.7, 134.1, 173.6.

**Table IV.1, entry 10**

**3-(2-Phenylethynyl)quinoline**[36]

Yellow solid, 65-68 $^{o}$C (Lit. mp 67-70 $^{o}$C)

IR (in KBr): $\nu_{max}$ 2218 cm$^{-1}$

$^1$H NMR ($CDCl_3$, 300 MHz): 7.38-7.41 (m, 3H, ArH), 7.55-7.61 (m, 3H, ArH), 7.70-7.76 (m, 1H, ArH), 7.79-7.82 (m, 1H, ArH), 8.12 (d, *J* = 8.4 Hz, 1H, ArH), 8.32 (d, *J* = 1.8 Hz, 1H, ArH), 9.00 (d, *J* = 1.8 Hz, 1H, ArH); $^{13}$C NMR ($CDCl_3$, 75 MHz): 86.4, 92.7, 117.5, 122.5, 127.3, 127.4, 127.6, 128.5, 128.8, 129.1, 130.2, 131.7, 138.5, 146.4, 151.9.

**Table IV.1, entry 12A**

**1-(2-(3-Bromophenyl)ethynyl)-4-methylbenzene**[37]

White crystalline solid, mp 91-93 $^{o}$C (Lit. mp 89-91 $^{o}$C)

IR (in KBr): $\nu_{max}$ 2222 cm$^{-1}$

$^1$H NMR ($CDCl_3$, 300 MHz): δ/ppm 2.37 (s, 3H, $OCH_3$), 7.14-7.25 (m, 3H, ArH), 7.40-7.46 (m, 4H, ArH), 7.67 (t, *J* = 1.8 Hz, 1H, ArH); $^{13}$C NMR ($CDCl_3$, 75 MHz): δ/ppm 21.5, 87.1, 90.9, 119.6, 122.1, 125.5, 129.1, 129.7, 130.0, 131.1, 131.5, 134.2, 138.8.

**Table IV.1, entry 12B**

**1-(2-(3-Biphenyl)ethynyl)-4-methylbenzene**

White Solid, mp 69-71 $^{o}$C

$^1$H NMR ($CDCl_3$, 300 MHz): δ/ppm 2.37 (s, 3H, $OCH_3$), 7.16 (d, *J* = 8.1 Hz, 2H, ArH), 7.36-7.53 (m, 8H, ArH), 7.59-7.62 (m, 2H, ArH), 7.76-7.77 (m, 1H, ArH); $^{13}$C NMR ($CDCl_3$, 75 MHz): δ/ppm 21.5, 88.7, 89.7, 120.2, 124.0, 126.9, 127.1, 127.6, 128.7, 128.8, 129.1, 130.3, 131.5, 138.4, 140.4, 141.4.

## IV.6. References

References are given in BIBLIOGRAPHY under Chapter IV (pp. 148−151).